On the long-term behavior of meandering rivers

C. Camporeale,[1] P. Perona,[2] A. Porporato,[3] and L. Ridolfi[1]

Received 14 March 2005; revised 26 August 2005; accepted 1 September 2005; published 1 December 2005.

[1] In spite of notable advances in the description of river morphodynamics, the long-term dynamics of meandering rivers is still an open question, in particular, regarding the existence of a possible statistical steady state and its scaling properties induced by the competing action of cutoffs and reach elongation. By means of extensive numerical simulations, using three fluid dynamic models of different complexity and analysis of real data from the Amazon, North America, and Russia, we show that the reach cutoffs, besides providing stability and self-confinement to the meander belt, also act as a dynamical filter on several hydrodynamic mechanisms, selecting only those that really dominate the long-term dynamics. The results show that the long-term equilibrium conditions are essentially governed by only one spatial scale (proportional to the ratio of the river depth and the friction coefficient) and one temporal scale (proportional to the square of the spatial scale divided by the river width, the mean longitudinal velocity, and the erodibility coefficient) that contain the most important fluid dynamic quantities. The ensuing statistical long-term behavior of meandering rivers proves to be universal and largely unaffected by the details of the fluid dynamic processes that govern the short-term river behavior.

Citation: Camporeale, C., P. Perona, A. Porporato, and L. Ridolfi (2005), On the long-term behavior of meandering rivers, *Water Resour. Res.*, *41*, W12403, doi:10.1029/2005WR004109.

1. Introduction

[2] Meandering rivers are dynamical systems far from equilibrium driven by complex linear and nonlinear processes. Their typical spatial and temporal patterns have shown clues of statistical equilibrium [*Howard*, 1984; *Liverpool and Edwards*, 1995; *Sun et al.*, 1996; *Stølum*, 1996, 1998], self-organized criticality [*Furbish*, 1991; *Stølum*, 1996, 1997], and fractal geometry [*Snow*, 1989; *Nikora et al.*, 1993; *Stølum*, 1998]. They can be assimilated to planar curves evolving under two contrasting actions: the continuous elongation induced by the local bend erosion, and the sudden and sporadic shortening due to cutoff events. The first action generates new reaches and is due to complex fluid dynamic mechanisms [*Parker et al.*, 1983; *Seminara*, 1998]. It also provides a spatial memory to the dynamics and gives rise to the sensitivity to initial conditions typical of locally (spatially or temporally) unstable systems [*Argyris et al.*, 1994]. The second action is intermittent and dictated by nonlocal geometric conditions that eliminate the most mature meanders when two points of the curve come into contact [*Gagliano and Howard*, 1984]. This sequence of elongation and shortening phases, which represents the core of the long-term dynamics of meandering rivers, is in turn impacted by several external forcings, such as flow variability, riparian vegetation, geological processes, and anthropic actions [e.g., *Sun et al.*, 1996; *Perona et al.*, 2002]. In the following, we will indicate as "long term" the timescale that includes cutoff occurrences, in contrast to the "short-term" timescale which is typical of the evolution of single meanders before cutoff.

[3] The present work deals with two aspects of the long-term dynamics. The first one is the possibility that a statistically stationary state may be reached by only two "internal" causes, that is, elongations and cutoff events, and not because of other "external" forcings. The previous results are somewhat contradictory to this regard. *Sun et al.* [1996] underline the necessity of the pedological processes for the self-confinement of the meander belt, while *Howard* [1984] and *Stølum* [1996] seem to obtain stationary states without introducing any external forcing. The second aspect concerns the role of cutoff in selecting the morphodynamic processes that are really important in the long-term dynamics. As will be seen, our results show that the shortening phases due to cutoff prevent several fluid dynamics mechanisms that are important in the short-term evolution from exerting a significant role in the long-term meandering dynamics. As a consequence, the overall complexity of the equilibrium state is markedly reduced and becomes essentially regulated by only two fundamental scales. Once normalized by such scales (that we obtain from fluid dynamic models and not empirically) the main features of the statistical steady state attain a clear universal character.

[4] The recognition of this "dynamic" filtering by cutoff is the principal novelty of the work. It also provides an interpretation for some well-known empirical laws of river geomorphology [*Leopold and Wolman*, 1960; *Jansen et al.*, 1979; *Allen*, 1984] whose evident scale invariance is apparently at odds with the complexity of

[1]Department of Hydraulics, Politecnico di Torino, Turin, Italy.
[2]Institute of Hydromechanics and Water Resources Management, Eidgenössische Technische Hochschule, Zurich, Switzerland.
[3]Department of Civil and Environmental Engineering, Duke University, Durham, North Carolina, USA.

0043-1397/05/2005WR004109$09.00

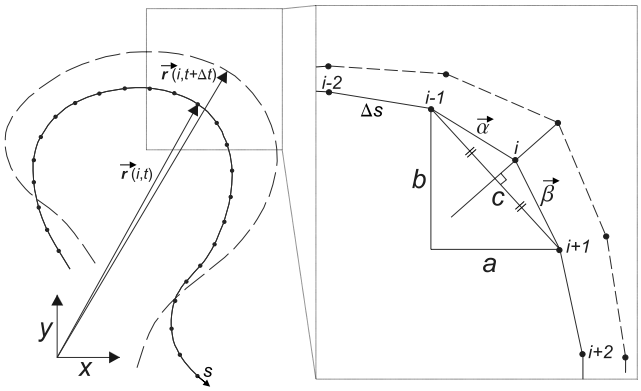

Figure 1. Geometric framework. Notice that $|\alpha| = |\beta|$.

the fluid dynamic mechanisms involved in the short-term meandering dynamics. It is in fact the occurrence of cutoffs that removes most of such a dynamic complexity and selects the few governing scales of the long-term dynamics.

[5] As the nonlinearity due to cutoff and its random occurrence prevent an analytical description of the long-term river dynamics, we thus employ numerical simulations of the temporal evolution of the river planimetry. We use a series of fluid dynamic models, namely the model of *Ikeda et al.* [1981], *Johannesson and Parker* [1989], and *Zolezzi and Seminara* [2001]. The first two models have been used in previous studies of long-term river dynamics [e.g., *Howard*, 1984; *Stølum*, 1996; *Sun et al.*, 1996, 2001], while the last one, which encompasses all the principal morphodynamic mechanisms, has never been used in long-term simulations. A recent investigation by the authors (C. Camporeale et al., Hierarchy of models for meandering rivers and related morphodynamic processes, submitted to *Reviews of Geophysics*, 2005, hereinafter referred to as Camporeale et al., submitted manuscript, 2005) has shown how such models can be hierarchically derived from a common framework by increasing the detail in the modeling of the fluid dynamic processes. Therefore the analysis of the long-term behavior of such models allows us to investigate the significance of each fluid dynamic process and to reveal the filtering action by cutoff in the long-term river dynamics.

[6] Finally, we support the results of the numerical simulations by analyzing the planimetric characteristics of forty four real rivers with very different hydraulic characteristics and spatial scales. We pay particular attention to the analysis of their scaling behavior and their meander belt characterization.

[7] The work is organized as follows. Section 2 is devoted to a brief review of the common mathematical framework used by the three models of the meandering dynamics. Section 3 deals with the numerical procedure adopted to simulate the long-term dynamics, while section 4 presents the simulation results along with a comparison with data from real rivers. Finally, section 5 draws the conclusions of our analysis.

2. Mathematical Framework

[8] The evolution of the river planimetry can be described using the formalism of the differential geometry of plane curves. Assuming that the width of the river remains constant during its migration, it is sufficient to study the evolution of the curve described by the river axis. The main steps for the deduction of the integrodifferential equation regulating the curve dynamics are the following (see *Nakayama et al.* [1992] and *Brower et al.* [1984] for more details). The starting point is the equation of motion of a parameterized curve $\mathbf{r}(\alpha, t)$ that moves along the normal versor $\mathbf{n}$ (see Figure 1), $\partial\mathbf{r}(\alpha, t)/\partial t = \mathbf{n}V$, where t is time, V is the local normal velocity, and α is a descriptive parameter which does not depend on time, so that $\partial_{t\alpha} = \partial_{\alpha t}$. Introducing then the arc length coordinate $s(\alpha, t) = \int_0^\alpha \sqrt{g}\,d\alpha'$, where $g(\alpha, t)$ is the metric coefficient $\left|\frac{\partial\mathbf{r}}{\partial\alpha}\cdot\frac{\partial\mathbf{r}}{\partial\alpha}\right|$, and defining the curvature $C = |\partial^2\mathbf{r}/\partial s^2|$, it follows that [*Brower et al.*, 1984]

$$\frac{\partial}{\partial t\partial s} - \frac{\partial}{\partial s\partial t} = -CV\frac{\partial}{\partial s}. \tag{1}$$

[9] Equation (1) along with the Serret-Frenet equations [*Do Carmo*, 1976] provides the temporal rate of change of the arc length coordinate

$$\frac{\partial s}{\partial t} = \int_0^\alpha \frac{\partial g}{\partial t}\frac{1}{2\sqrt{g}}d\alpha' = \int_0^\alpha \frac{gCV}{\sqrt{g}}d\alpha' = \int_0^s CVds', \tag{2}$$

which gives [*Nakayama et al.*, 1992]

$$\frac{d\mathbf{r}}{dt} = \mathbf{n}V - \frac{\partial\mathbf{r}}{\partial s}\int_0^s CVds'. \tag{3}$$

Once the normal velocity, $V(s, t)$, is given, the previous equation describes univocally the dynamics of the curve. Notice that equation (3) is nonlinear, regardless of the mathematical form of V.

[10] In the case of meandering rivers, the functional V can be modelled following an original idea of *Ikeda et al.* [1981] who suggested a linear relationship between the normal rate of erosion and excess bank longitudinal velocity $u_b = u(s, n = b)$, that is, $V = E \cdot u_b$, where $u(s, n)$ is the longitudinal flow field perturbation to the mean stream velocity, n is the transversal coordinate, b is the river half width, and E is a coefficient of erodibility (a complete list of symbols is provided at the end of the paper). Such a hypothesis was confirmed by field investigations [*Pizzuto and Meckelnburg*, 1989] and has been adopted in several models for its simplicity [*Parker and Andrews*, 1986; *Johannesson and Parker*, 1989; *Odgaard*, 1986; *Howard*, 1992]. It should be noted that u_b refers to the value at the edge of the lateral boundary layer and thus it corresponds to the velocity given by the two-dimensional theories describing the flow field in meandering rivers. In particular, in this paper we adopt the models developed by *Ikeda et al.* [1981], by *Johannesson and Parker* [1989], and by *Zolezzi and Seminara* [2001] (hereinafter referred to as IPS, JP, and ZS models, respectively). While a detailed comparison among the models has been conducted elsewhere (Camporeale et al., submitted manuscript, 2005), here we only recall some essential physical properties and their conceptual differences.

[11] As shown by Camporeale et al. (submitted manuscript, 2005), these three theories can be hierarchically derived from the same framework (i.e., the shallow water equations and the continuity equation for the sediment) and differentiate themselves according to the morphodynamic mechanisms considered. In the case of the ZS model, the generic m mode of the lateral Fourier decomposition of the longitudinal flow field perturbation, $u(s, n) = \sum_{m=0}^{\infty} u_m(s) \sin Mn$ (with n transversal coordinate and $M = \frac{1}{2}[(2m + 1)\pi]$, is described by the following fourth-order linear differential equation

$$\frac{d^4u_m}{ds^4} + \hat{\sigma}_3\frac{d^3u_m}{ds^3} + \hat{\sigma}_2\frac{d^2u_m}{ds^2} + \hat{\sigma}_1\frac{du_m}{ds} + \hat{\sigma}_0 u_m = \sum_{j=0}^{6}\hat{\rho}_j\frac{d^jC}{ds^j}. \quad (4)$$

[12] The coefficients of the above equation read

$$\hat{\sigma}_i = \frac{\sigma_i b}{\nu_0 U_0}, \qquad \hat{\rho}_j = A_m b \rho_j \qquad (i = 1,4; j = 0,6), \quad (5)$$

where $A_m = 2(-1)^m/M^2$, $\nu_0 = b/R_0$, R_0 is the minimum radius of curvature of the river, U_0 is the bulk velocity, and the terms σ_i and ρ_i depend on the aspect ratio $\beta = b/H$, the dimensionless roughness $d_s = d_m/H$ and the Shield stress θ (for details see *Zolezzi and Seminara* [2001]). Finally, H is the average depth and d_m the mean sediment diameter.

[13] Equation (4) provides the most complete linear fluid dynamics-based solution of the river morphodynamic problem. It contains some fundamental novel aspects to the previous linear formulations. First, the ZS model fully accounts for the coupling between curvature-driven secondary currents and topography-driven secondary flow, by considering the redistribution of the secondary flow through the action of the main flow. The fourth order of the equation (4) arises from the dependence of the free surface on both these components of the lateral flow. Secondly, the two complex conjugate eigenvalues that are always present in the solutions of the secular equation corresponding to the free response of the system, cause an oscillatory pattern in the flow field that allows the modeling of multilobed behavior in the curve growth [*Seminara et al.*, 1994]. Thirdly, the model accounts for the spatial change in the friction factor as well as for the vertical variation of the eddy viscosity by means of Dean's distribution [*Dean*, 1974], which may strongly influence the normal rate of erosion (Camporeale et al., submitted manuscript, 2005). Finally, since one eigenvalue is always positive, the ZS model reveals that the local flow field depends on both the upstream and downstream river geometry. The former dependence becomes dominant in the so-called superresonant conditions giving rise to upstream-skewed meanders.

[14] The JP model can be obtained from the ZS model with three main simplifications: (1) negligible coupling between curvature driven secondary currents and topography, (2) no spatial variations in the friction coefficient and no dependence of the bedload transport on the flow depth, and (3) vertically averaged value of the eddy viscosity. With the previous assumptions, equation (4) reduces to the second-order model

$$\frac{d^2u_m}{ds^2} + \sigma_1'\frac{du_m}{ds} + \sigma_0' u_m = \sum_{j=0}^{2}\rho_j'\frac{d^jC}{ds^j}, \quad (6)$$

whose first lateral mode ($m = 0$) corresponds to the JP model. Coefficients σ_i' and ρ_i' are reported in appendix A.

[15] If we further neglect the coupling between sediment dynamics and fluid dynamics and model the dimensionless bed elevation $\eta(n, s)$ through the linear relationship $\eta = -ACn$ (where A is a coefficient depending on the friction factor and the turbulence closure model), equation (6) solved at the wall (i.e., $u_b = u(s, n = b)$) reduces to a first-order equation

$$\frac{du_b}{ds} + \sigma_0'' u_b = \rho_0'' C + \rho_1''\frac{dC}{ds}. \quad (7)$$

[16] This corresponds to the IPS model, which can be considered as the founder of the physically based meandering models (for the coefficients σ_i'' and ρ_i'', see *Ikeda et al.* [1981] and *Sun et al.* [1996]). In spite of its several simplifying hypotheses, it captures some of the fundamental features of the meandering dynamics, like the fattening and the skewing in meander evolution. This fact, together with the model simplicity, explains the use of the IPS model in several theoretical and numerical works [e.g., *Parker et al.*, 1983; *Beck*, 1984; *Parker and Andrews*, 1986; *Sun et al.*, 1996].

3. Numerical Algorithm

[17] The long-term dynamics of meandering rivers was investigated by numerical simulations of the three meandering models ZS, JP, and IPS, with different hydraulic conditions. Each simulation started from a straight line with weak random perturbations to trigger instability. Each simulation was carried out using the following iterative algorithm.

3.1. Step One

[18] The river axis is discretized as a sequence of points i ($i = 1,.., N$) with a constant spacing Δs by means of a spline interpolation (see Figure 1). We chose $\Delta s = b/4$. In each point, the local curvature is then evaluated according to

$$C = -\frac{\partial\phi}{\partial s} \simeq -\frac{(\arcsin\boldsymbol{\alpha}\wedge\boldsymbol{\beta})}{|\boldsymbol{\alpha}||\boldsymbol{\beta}|\Delta s} = \frac{\alpha_y\beta_x - \alpha_x\beta_y}{\Delta s^3}, \quad (8)$$

where ϕ is the angle between the local tangent to the river axis and the x coordinate, and $\boldsymbol{\alpha} = (\alpha_x, \alpha_y)$ and $\boldsymbol{\beta} = (\beta_x, \beta_y)$ are the vectors reported in Figure 1. The endpoints of the river (i.e., $i = 1, N$) were set to have zero curvature.

3.2. Step Two

[19] The longitudinal flow field and $u_b(s)$ are evaluated from the corresponding mathematical models. For the JP and IPS models this was done by solving the equations (6) and (7) by means of a fourth-order Runge-Kutta scheme, while the presence of a the positive eigenvalue in the ZS model requires a different procedure. We thus used the solution reported by *Zolezzi and Seminara* [2001] which

Table 1. Morphodynamic Parameters Used in the Simulations

Run	d_s	θ	β	C_{f0}	D_0, m	T_0, years	Q, m^3 s^{-1}	$\bar{\lambda}$, m[a]
S_1	0.025	0.18	14.6	0.0060	45	105	23	728
S_2	0.020	0.10	15.4	0.0054	77	211	50	1023
S_3	0.012	0.10	15.1	0.0045	123	422	85	1550
S_4	0.012	0.10	13.4	0.0036	153	528	132	2050
S_5	0.006	0.30	14.6	0.0032	250	634	382	3214
S_6	0.004	0.40	14.0	0.0032	250	792	271	3050
S_7	0.008	0.15	13.1	0.0040	250	792	334	3190
S_8	0.010	0.20	15.8	0.0043	450	635	2621	5854
S_9	0.010	0.20	13.4	0.0043	500	792	2877	6545
S_{10}	0.004	0.40	14.8	0.0032	500	1058	1630	6610

[a]Mean of results obtained using IPS, JP, and ZS models.

consists of a local term, four boundary conditions, and four convolution integrals that can be written as

$$I_j = \int_a^b e^{\epsilon_j(s-z)} C(z)dz \qquad (j = 1, 4), \tag{9}$$

where ϵ_j are the four eigenvalues of the secular equation and $(a, b) = (s, 0)$ for $j = 1$ and $(a, b) = (0, s)$ for $j = 2, 3, 4$. The evaluation of the integrals (9) requires great care as explained in Appendix B. However, even if the high decay rate of the exponential in the integrals I_j at higher Fourier modes m (due to the increment of $|\epsilon_j|$ with m) would require very small Δs to maintain the same precision for all modes, the influence of the convolution integrals on u_b becomes negligible at higher modes. As a consequence, as verified with several numerical tests, it was sufficient to consider only the first two modes maintaining the same spatial discretization. The same numerical tests suggested that the computation of the curvature derivatives involved in the known term of (4) can be stopped at the third order, being the coefficients ρ_{4-6} negligible.

3.3. Step Three

[20] Once the excess bank longitudinal velocities are computed for the three models, the points of the curves have to be shifted normally to the local tangent (see Figure 1) according to the evolution equation (3). To this aim we adopted a geometrical method that takes advantage of the uniformity of the distances Δs between points to give

$$x_i(t + \Delta t) = x_i(t) - \zeta \frac{b}{c}; \quad y_i(t + \Delta t) = y_i(t) + \zeta \frac{a}{c}, \tag{10}$$

where $x_i(t)$ and $y_i(t)$ are the coordinate of the ith point at the time t, Δt is the temporal step, $\zeta = V\Delta t = Eu_b\Delta t$ is the normal displacement, $a = [x_{i+1}(t) - x_{i-1}(t)]$, $b = [y_{i+1}(t) - y_{i-1}(t)]$, and $c = \sqrt{a^2 + b^2}$. The ratio $\Delta s/\Delta t$ was maintained of order 10^{-4} m/s to ensure the curve smoothness, as pointed out by [*Seminara et al.*, 2001]. As $\Delta s = b/4$ and the river width is usually 10^1–10^2 m, the time step Δt is of the order of a few days.

3.4. Step Four

[21] The fourth step concerns the search for potential cutoff events along the river. A neck cutoff happens whenever two points of the rivers come into contact. As we are only following the evolution of the river axis, this would imply considering a threshold value equal to the river width, b. However, a larger and more realistic value of the threshold can be reasonably used [*Howard*, 1992]; so, we adopted a threshold equal to 1.5 times the river width. It is evident that this choice does not consider the chute cutoffs, but a correct modeling thereof would require a probabilistic approach coupled with the description of the evolution of floodplain topography and riparian vegetation, and this is outside the scope of the present work. On the other hand, such a conservative value allows the river to develop quite a high sinuosity, and thus the different dynamic characteristics of the models to clearly emerge during the meanders elongation phases (we will come back to this point in the following).

[22] To identify the points closer than the selected threshold we used the matrix algorithm explained in Appendix C. Such a searching method is much more efficient than those previously used [e.g., *Sun et al.*, 1996, 2001; *Stølum*, 1997] and it is thus particularly useful for long-term simulations. Once the possible cutoff is detected, the points of abandoned reach are deleted, assuming that they no longer play any role in the dynamics. The algorithm then goes back to the first step and the procedure is iterated.

4. Analysis and Results

4.1. Long-Term Simulations

[23] Table 1 reports the ten hydraulic configurations that have been considered for the simulations with the three mathematical models, ZS, JP, and IPS. These cover very different morphodynamic conditions within the subresonant regime [*Zolezzi and Seminara*, 2001] of meander formation range proposed by *Parker* [1976]. The soil erodibility coefficient, E, was fixed equal to $3 \cdot 10^{-8}$ for all the simulations [*Beck et al.*, 1984; *Sun et al.*, 1996], without loss of generality. As will be seen, in fact, the value of E only changes the timescale of the meandering process, leaving the spatial characteristics unaltered.

[24] In order to obtain statistically significant results, the length of the initial straight line was varied from 10 km for the smallest river (S_1) to 100 km for the biggest one (S_{10}), while the corresponding duration of the simulations ranged from 10^3 and 10^5 years. The total number of points N was about 10^3 for a maximum number of iterations of about 10^7.

[25] During each simulation, we followed the dynamics of the river planimetry focusing on the temporal evolution

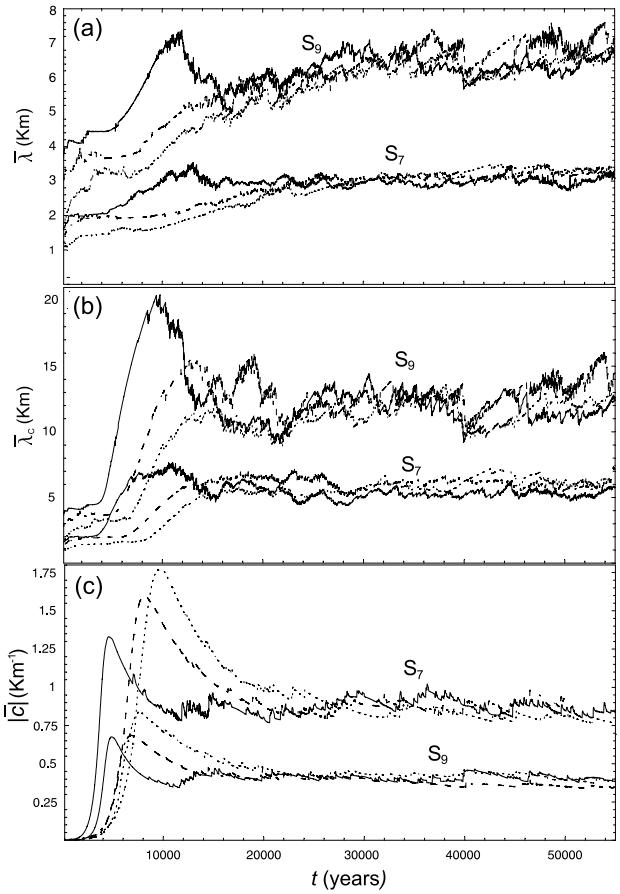

Figure 2. Evolution of (a) the river mean wavelength, (b) the mean curvilinear wavelength, and (c) the mean absolute curvature for simulations S_7 and S_9, (dotted line, IPS model; dashed line, JP model; solid line, ZS model).

of the sinuosity, S, the tortuosity τ, the probability density functions (pdfs) of the linear and curvilinear wavelengths (λ and λ_c respectively), and the pdf and the autocorrelation of the local curvatures along the river. The sinuosity is defined as the ratio between the river length and the length of the broken line joining the inflection points. The tortuosity is defined as the ratio of the river length to the linear distance between its endpoints. The linear wavelength is assumed equal to twice the linear distance between the zero crossings of the curvature, while the curvilinear one refers to the distance along the river [e.g., *Allen*, 1984].

[26] Figure 2 shows the evolutions of the mean wavelength, $\bar{\lambda}$ (the overbar refers to the spatial averaging), the mean curvilinear wavelength, $\bar{\lambda}_c$, and the mean absolute curvature, $|\bar{C}|$. They refer to two hydraulic conditions, each simulated using the three different models. We can easily distinguish three phases in the river evolution. A first phase takes place before the occurrence of cutoffs, where strong differences among the models are evident, due to the different fluid mechanic processes included in the modeling. A second phase sets in when cutoffs start to appear and the differences between the models tend to phase out. Finally, a third phase occurs when a statistically steady state (that is substantially independent of the morphodynamic model adopted) is attained. This type of evolution that is common to all the other geometric quantities analyzed in all the simulations represents the key point of our analysis.

[27] The statistically steady state reached by the long-term river geometry (Figure 2) is controlled by the sole action of the internal dynamics of elongation and cutoff. Thus the external forcings (e.g., geological constraints, pedological processes, riparian vegetation dynamics, etc.), although influencing the steady state in real rivers, are not necessary to obtain it. This confirms the results of previous investigations [*Howard*, 1984; *Liverpool and Edwards*, 1995; *Stølum*, 1996] and clearly shows that cutoffs are sufficient to give stochastic stability to the system (i.e., self-confinement of the meander belt; see subsection 4.3), independently of the fluid dynamic model used to describe the elongation phases (i.e., the erosion rate, V).

[28] The convergence to a model-independent steady state implies that the most simplified (but physically based) meandering model (i.e., the IPS model) already contains all the necessary ingredients to describe the long-term dynamics. Some of the fluid dynamic processes described by the more complex models (in particular the ZS model) do not exert any relevant influence on the statistical properties of the long-term steady state (at least those investigated here). The sequence of the three phases observed in Figure 2 clearly suggests that the cutoff is responsible for such a dynamical simplification. By removing the oldest river reaches, the cutoffs lead to a progressive elimination of the cumulated geometric differences resulting from the use of different morphodynamic models and leave only the essential dynamical characteristics common to all models.

[29] Notwithstanding the statistical similarity among the long-term simulations, it should be noticed that the single instantaneous planimetric configurations at steady state can be also very different among the models. An example,

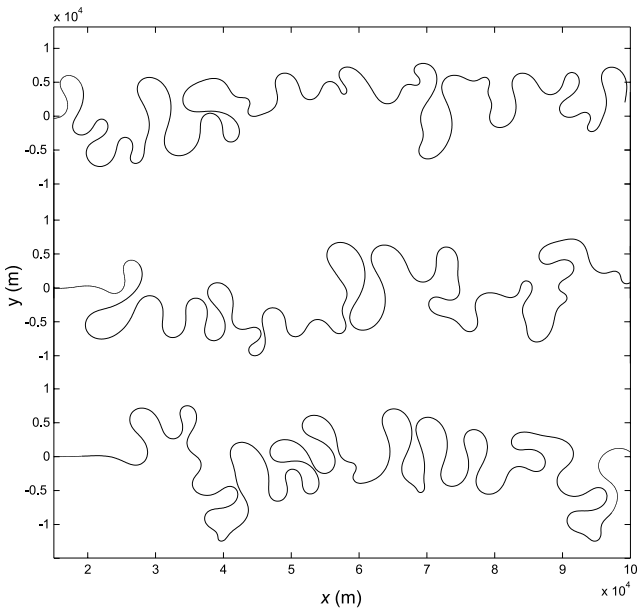

Figure 3. Configuration at time t = 30,000 years for (top) IPS, (middle) JP, and (bottom) ZS model, run S_{10}.

Table 2. Rivers Considered in the Analysis[a]

Rivers	$\bar{\lambda}$, m	$\bar{\lambda}_c$, m	$\tau^{1/3}$
Walla Walla (Washington)	194	267	1.88
Johnson-2 (Yukon Territory)	367	521	1.29
Johnson-1 (Yukon Territory)	393	593	1.23
Porcupine (Yukon Territory)	408	616	1.37
Johnson-3 (Yukon Territory)	435	677	1.31
Man (Manitoba)	459	661	1.39
Assiniboine (Manitoba)	485	744	1.35
Little Black (Alaska)	490	767	1.45
Johnson-4 (Yukon Territory)	496	690	1.29
Hodzana (Alaska)	757	1231	1.39
White-1 (Indiana)	792	1530	1.20
Birch-1 (Alaska)	844	1342	1.42
Old Crow-1 (Yukon Territory)	935	1381	1.47
Black-1 (Alaska)	982	1367	1.39
Birch-2 (Alaska)	994	1525	1.34
White-2 (Indiana)	1001	1629	1.36
Birch-3 (Alaska)	1002	1477	1.36
Pembina (Alberta)	1021	1576	1.41
Koyukuk-1 (Alaska)	1185	1914	1.38
Old Crow-2 (Yukon Territory)	1233	1846	1.34
Black-2 (Alaska)	1450	2177	1.31
Purus-1 (Brazil)	1804	2656	1.29
Purus-3 (Brazil)	1866	2585	1.34
Purus-2 (Brazil)	2030	2872	1.26
Purus-4 (Brazil)	2192	2902	1.31
Jurua-3 (Brazil)	3432	4518	1.27
Koyukuk-2 (Alaska)	3542	5349	1.30
Jurua-2 (Brazil)	3762	5105	1.27
Jurua-1 (Brazil)	3815	6167	1.39
Jurua-4 (Brazil)	4124	6178	1.33
Jurua-5 (Brazil)	4312	6767	1.32
Koyukuk-4 (Alaska)	4676	8043	1.31
Markha-1 (Russia)	4692	6488	1.25
Markha-3 (Russia)	5088	6522	1.36
Koyukuk-3 (Alaska)	5163	7065	1.31
Purus-5 (Brazil)	5561	8362	1.30
Markha-2 (Russia)	6223	9634	1.22
Purus-6 (Brazil)	6605	10190	1.35
Ucayali-1 (Peru)	7057	9875	1.27
Purus-7 (Brazil)	7272	12000	1.18
Ucayali-3 (Peru)	7275	10918	1.31
Ucayali-4 (Peru)	8567	12359	1.23
Ucayali-2 (Peru)	8707	14183	1.28
Purus-8 (Brazil)	8963	13283	1.35

[a]The number after the name refers to different reaches of the same river.

corresponding to the same initial condition, is shown in Figure 3. Thus the long-term statistical spatial properties investigated here must not be confused with the details of the single planimetry that reflect the short-term evolution and thus the fluid dynamic differences between models, such as the role of the turbulence closure, the presence of higher harmonics, and the spatial distribution of the friction factor (Camporeale et al., submitted manuscript, 2005).

[30] The fact that the IPS model is sufficient to fully describe the steady state statistical properties also implies that the same dimensionless groups proposed by *Edwards and Smith* [2002] for the short-term dynamics of such a model can also be used for the long-term dynamics including the cutoffs. These groups can be obtained starting from the formal solution of the IPS model [*Sun et al.*, 1996],

$$u_b = -bUC + \frac{UbC_f}{H}\left[F^2 + A + 1\right]\int_{-\infty}^{s} e^{-\frac{2C_f}{H}(s-z)}C(z)dz, \quad (11)$$

where U is the mean stream velocity, C_f is the friction factor, F is the Froude number, and A is the lateral slope factor. Applying dimensional analysis to (3) and (11), the essential geometric and hydraulic parameters can be used to form a spatial scale $D = H/2C_f$ and a temporal scale $T = D^2/bU\,E$. Notice that the dimensionless ratio of the stress term to the convective term in the St Venant shallow water equations reduces to H/LC_f (where L is a generic length scale); it follows that the scale D is close to the backwater length H/I, with I the overall bed slope. The role of the temporal scale T is apparent in the transient phase, while the spatial scale D impacts the statistically steady state properties through its influence on the kernel of the convolution integral of (11) that in turn controls the downstream influence of the curvature on the local river displacement. Moreover, once scaled with the time-independent values D_0 and T_0 (the subscript refers to the "straightened" river), the dimensionless rate of bank erosion, $\tilde{V} = u_b E T_0/D_0$, satisfies the following linear differential equation [*Edwards and Smith*, 2002]

$$\tau^{1/3}\frac{\partial \tilde{V}}{\partial \tilde{s}} + \tilde{V} = \frac{\partial \tilde{C}}{\partial \tilde{s}} + \frac{P}{\tau^{1/3}}\tilde{C}, \quad (12)$$

where the tilde refers to dimensionless quantities, while τ is the tortuosity defined before, and $P = (F^2 + A + 1)/2$ is a parameter that depends on sediment dynamics. Both simulations and real data (Table 2) show that the variance of the steady state values of $\tau^{1/3}$ is about 10^{-3}–10^{-2} regardless of the hydraulic characteristics. This has been also confirmed by the comparison with the tortuosity time series reported by *Stølum* [1996] and with the data of *Howard and Hemberger* [1991]. Similarly, it can be shown that the parameter P has also a negligible influence on equation (12). As a result equation (12) turns out to be essentially controlled by only D_0 and T_0 without need to use the tortuosity-dependent scales $D = \tau^{1/3}D_0$ and $T = \tau T_0$.

[31] After normalization with D_0 and T_0, the results of the simulations of the three models for different hydraulic conditions (i.e., $10 \times 3 = 30$ simulations) collapse on a common behavior characterized by $\bar{\lambda} \simeq 13.4D_0$, $\bar{\lambda}_s \simeq 25D_0$, and $|\bar{C}| \simeq 0.2/D_0$ (Figure 4). A similar collapse is obtained for the pdfs and the autocorrelation functions. Their envelopes (rescaled with D_0) are marked by two red lines in the Figure 5. As explained before, this universal behavior emerges as a symptom of the action of the cutoff in selecting the two governing scales D_0 and T_0 among various fluid dynamic mechanisms.

[32] The emergence of a fluid dynamic spatial scale, rather than a morphodynamic one, can be justified by noticing that in the context of the long-term evolution only the scale $D_0 = H_0/2C_{f0}$ influences the exponential factor of the convolution integrals (9) of the various models, despite the different hydrodynamic processes considered. This property is immediately evident in the IPS solution (see equation (11)), but may be also shown for ZS and JP models. In fact, each eigenvalue, ϵ_j, in the convolution integrals I_j can be written as the sum of two terms, $\epsilon_j = f_j(D_0) + g_j(\beta, \theta, d_s)$, where the first only depends on the scale D_0 ($g_j = 0$ for the IPS model). As the phase response of all the models is substantially the same (Camporeale et al., submitted manuscript, 2005), a single eigenvalue ϵ^*

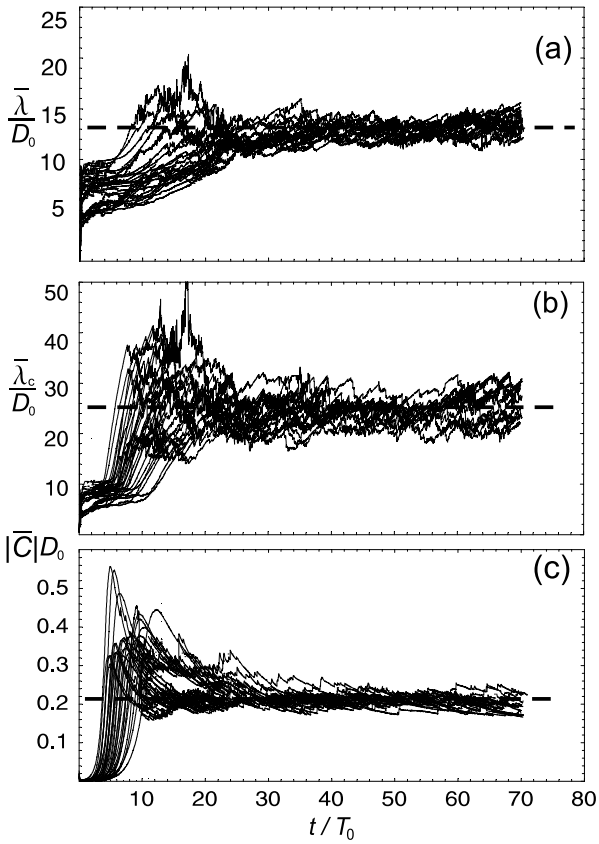

Figure 4. Evolution of (a) the river mean wavelength, (b) the mean curvilinear wavelength, and (c) the mean absolute curvature nondimensionalized with D_0 and T_0 for different hydraulic conditions using all three models (D_0 and T_0 range in the intervals [45, 500] m and [100, 1000] years, respectively).

controls the free response of the system and $g^* \ll f^*$. Consequently, since u_b is the main ingredient of the evolution equation (3), D_0 regulates the spatial response of meandering dynamics (i.e., the prevailing harmonic ϵ^*). The other sediment and fluid dynamic processes are contained in some multiplicative coefficients of the evolution equation and only affect the timescale of the dynamics at timescales that are larger than the time to reach cutoff. As a result, the dominant action of the cutoff overwhelms the effect of the higher harmonics related to the eigenvalues $\epsilon_j \neq \epsilon^*$ that therefore are not able to contribute to the long-term statistical properties.

4.2. Link With Empirical Laws

[33] The universal behavior obtained using the scale D_0 is in substantial agreement with some empirical geomorphologic laws. The reason for the good scaling of such empirical laws is probably due to the choice of quantities that contain D_0 or that directly depend on it. For example, the well-known Hansen's law [*Hansen*, 1967; *Jansen et al.*, 1979], $\bar{\lambda} = 14H_0/f$ (where f is the friction factor of Darcy-Weisbach), which is in very good agreement with the results of Figure 4 and thus confirms the reliability of the simulations, can be written in terms of D_0 as $\bar{\lambda}/D_0 = 14$.

[34] More recently, *Parker and Johannesson* [1989] reported the dimensionless ratio

$$\frac{Hk}{bC_f} = \frac{2\pi b}{\bar{\lambda}}\frac{2D}{b} = 4\pi\frac{D}{\bar{\lambda}} = O(1), \tag{13}$$

where k is the wave number made dimensionless with b. Such a relationship implies a ratio between $\bar{\lambda}$ and D of about 13, which is very close to the value of the Hansen's law. For example, previous theoretical works [*Parker and Andrews*, 1986; *Parker and Johannesson*, 1989] report the values of $H = 1$ m and $C_f = 0.0064$ for the Pembina River, from which we can evaluate a ratio $\bar{\lambda}/D_0 = 13.1$. Also, the results reported in Table 1 are also in agreement, with a relative mean error of 13%, with the empirical law $\bar{\lambda} = 170Q^{0.46}$ (Q is the mean annual discharge) proposed by *Carlston* [1965].

[35] The one-to-one link between D_0 and $\bar{\lambda}$ indicates that $\bar{\lambda}$ has the same physical meaning of D_0 and thus justifies the use of $\bar{\lambda}$ in place of D_0 as a characteristic length scale. This explains the good collapse obtained in some empirical geomorphologic laws using $\bar{\lambda}$ (e.g., the celebrated formula $\bar{\lambda} = 4.7\bar{r}^{0.98}$ of *Leopold and Wolman* [1960] where $\bar{r}$ is the mean radius of curvature). The use of $\bar{\lambda}$ has the advantage that, in practical applications, it can

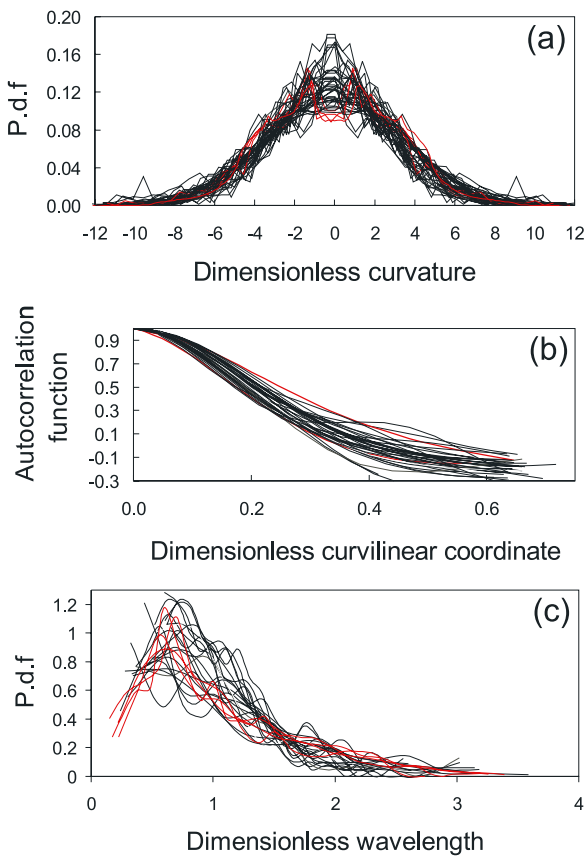

Figure 5. Scaling of physical quantities characterizing the river geometry with $\bar{\lambda}$: (a) pdfs of the curvatures, (b) autocorrelation functions of the curvatures, and (c) pdfs of the river wavelength. The black lines refer to data from real rivers, while the red lines mark the envelope of the curves obtained by simulated rivers.

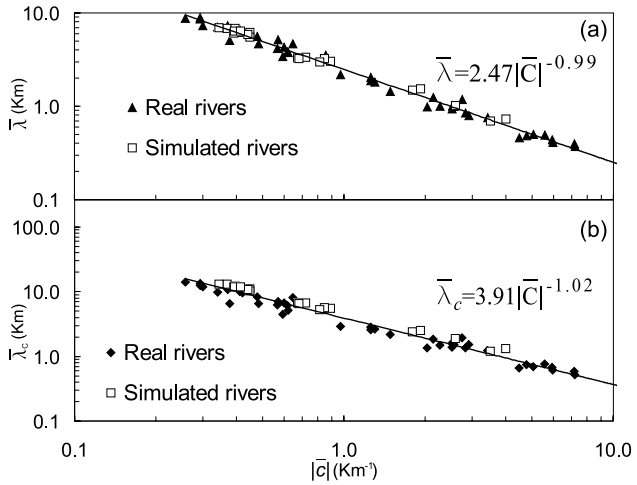

Figure 6. Links among the mean curvilinear wavelength, $\bar{\lambda}_c$, the mean wavelength, $\bar{\lambda}$, and the mean absolute radius of curvature (obtained by averaging the local values along the river) for both real and simulated rivers. The straight lines highlight the scale invariance (i.e., a power law dependence).

be rather easily estimated using remote sensing techniques, whereas the hydraulic parameters, and in particular the dominant discharge, make it difficult to estimate D_0. For this reason in what follows we make use of $\bar{\lambda}$ for the comparison with data from real rivers. Finally, we note that the bed width, $2b$, used as a typical length scale in some geomorphological laws [*Leopold et al.*, 1964; *Jansen et al.*, 1979], is closely related to the same hydraulic characteristics that are contained in D (or D_0). Therefore, since D_0 captures the fluid dynamic mechanisms that regulate the long-term dynamics, b too is a physically justified parameter to scale the planimetry river geometry.

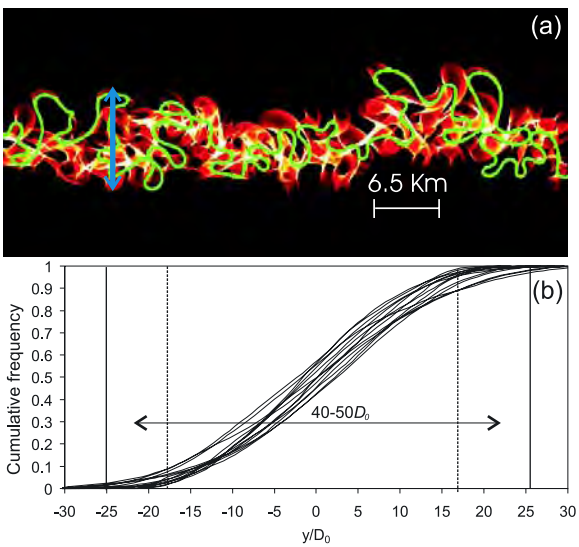

Figure 7. Probabilistic characterization of the meander belt. (a) Example of the frequency of the riverbed occurrence during the steady state (ZS model, D_0 = 250 m, T_0 = 600 years, and $\bar{\lambda}$ = 3250 m). The darkest shade refers to the lowest frequency, the green line marks the planimetry of the river at a generic time, and the blue arrow corresponds to $3.4\bar{\lambda}$. (b) Cumulative frequency of river occurrence at steady state for some simulated rivers (y is the coordinate transversal to the chord linking the river extremes).

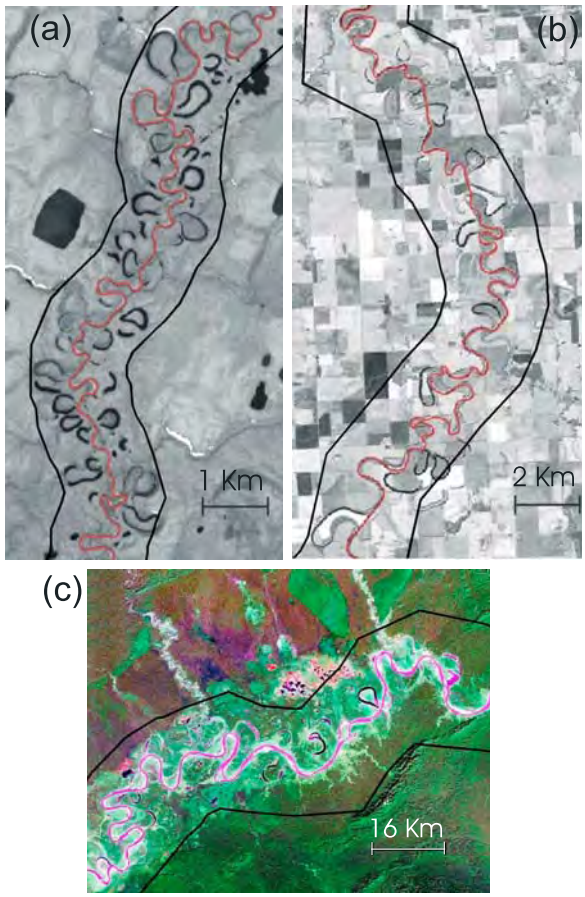

Figure 8. Planimetries of (a) Johnson Creek, (b) Pembina River, and (c) Ukayali River rescaled using their mean wavelength (equal to 435, 1021, and 7275 m, respectively); the bold black lines mark width equal to $3.4\bar{\lambda}$.

4.3. Comparison With Data From Real Rivers

[36] We validated the universal behavior of simulated river patterns using data from maps of Amazonian, North American, and Russian rivers with minimal anthropic perturbations. Forty-four reaches covering a wide range of wavelengths have been considered (see Table 2). The real data were obtained following the recommendations specified by *Howard and Hemberger* [1991] and consist of segments with nearly uniform discharge [see also *Stølum*, 1998].

[37] The same geometrical quantities used to analyze the simulated rivers were evaluated for the real rivers. Figure 5 shows the excellent agreement of the simulated and real pdf and autocorrelation of the curvatures as well as of the pdf of the meander wavelength, underlining the universal features in the long-term river geometry. In particular, since the pdf and the autocorrelation function completely define the linear properties of a process [*Kantz and Schreiber*, 1997], their remarkable collapse here implies the universality of all the linear geometric characteristics of meandering rivers [*Perucca et al.*, 2005]. In Figure 5b, the autocorrelation

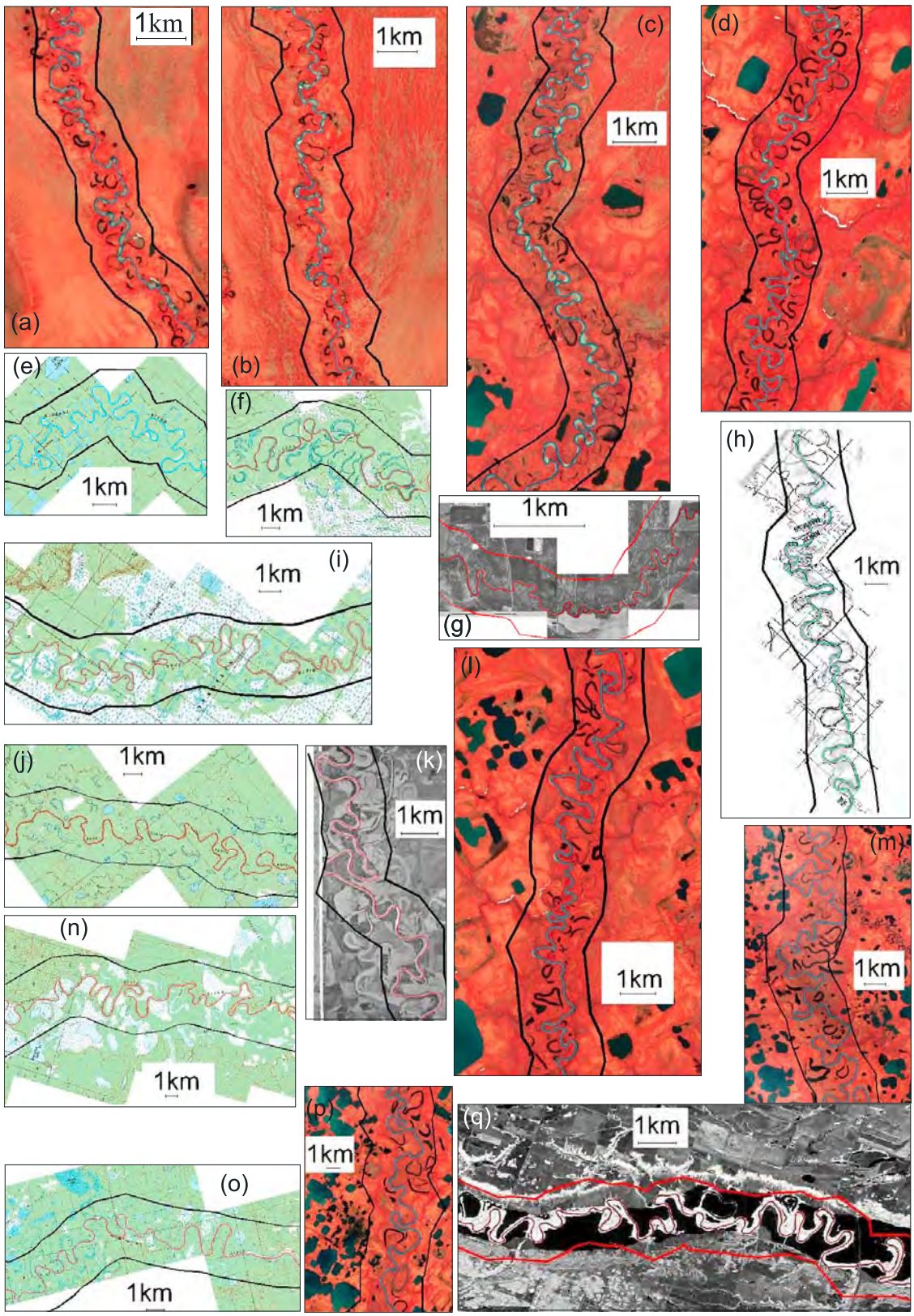

Figure 9. Rivers (a) Johnson-2, (b) Johnson-1, (c) Porcupine, (d) Johnson-1, (e) Hodzana, (f) Birch-2, (g) Walla Walla, (h) White, (i) Birch-1, (j) Little, (k) Assainboine, (l) Johnson-4, (m) Old Crow-1, (n) Black-1, (o) Black-2, (p) Old Crow-2, and (q) Man.

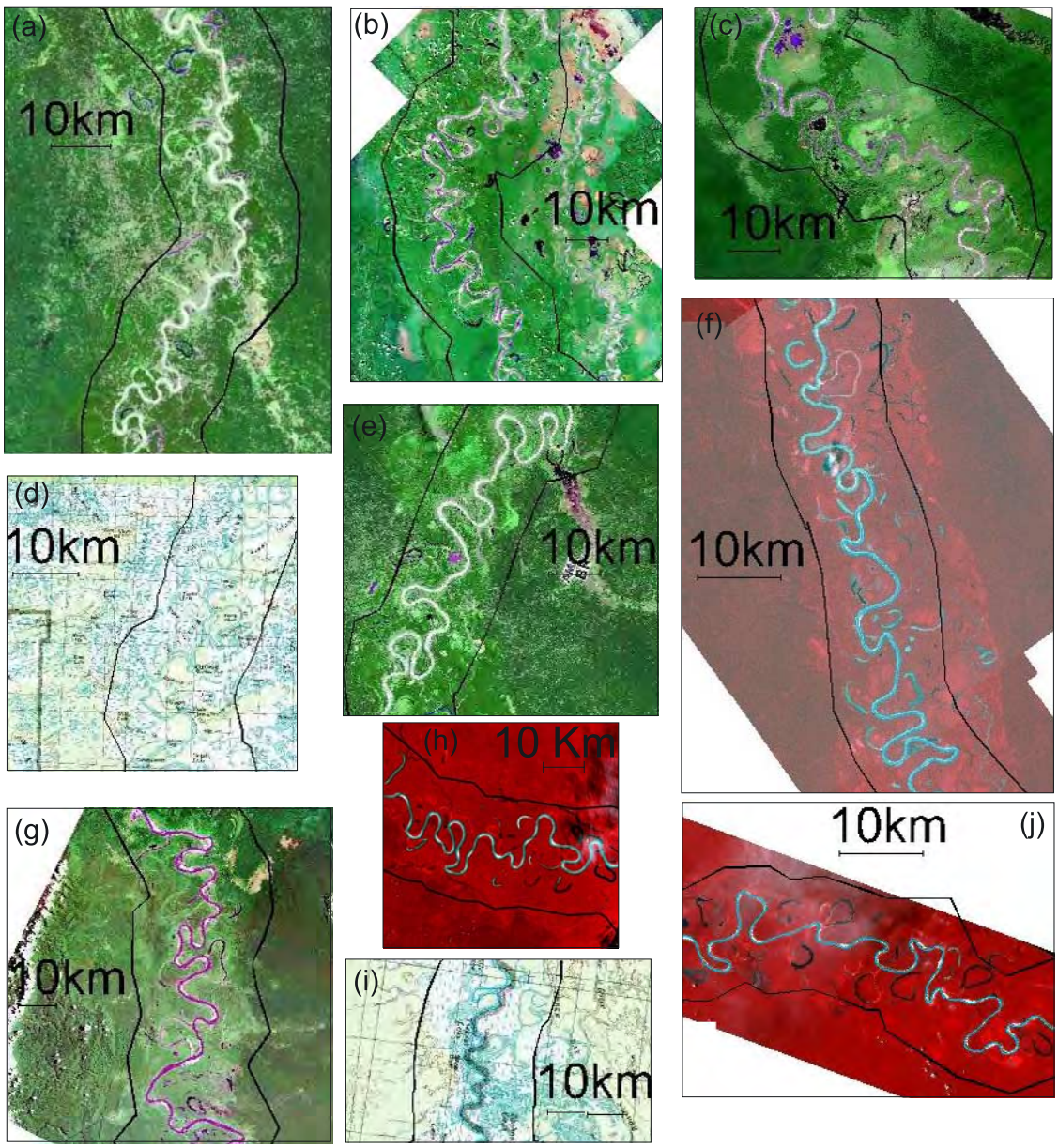

Figure 10. Rivers (a) Purus-5, (b) Ukayali-3, (c) Purus-7, (d) Koyukuk-3, (e) Purus-6, (f) Juruá-4, (g) Ukayali-2, (h) Purus-8, (i) Koyukuk-4, and (j) Juruá-5.

function suggests a typical integral scale of about 0.2 with a decay at about two fifth of the meander wavelength. Therefore the long-term "geometric" memory of the river is about 4–5 times larger than the "fluid dynamic" one represented by D_0. Figure 6 reports the links among the mean curvilinear wavelength, $\bar{\lambda}_c$, the mean wavelength, $\bar{\lambda}$, and the mean absolute curvature, $|\bar{C}|$. One can see the very good agreement among real and simulated rivers and a remarkable collapse on power laws, coherently with the empirical formula by *Leopold and Wolman* [1960]. To this regard, we note that differently from Leopold and Wolman who studied the link between $\bar{\lambda}$ and the mean radius of curvature, $\bar{r}$, measured from topographic maps, we used the mean absolute curvature, $|\bar{C}|$, to avoid overflow in the computation of the mean radius of curvature at the inflection points from high-precision digital maps. To compare our result to their formula we assumed $\bar{r} \cong 1/|\bar{C}|$, and this approximation explains the different value of the coefficient in the power laws.

4.4. Analysis of the Meander Belt

[38] A correct and general characterization of the meander belt is of great relevance for flood management, riparian restoration, and oil deposit research [*Swanson*, 1993; *Sun et al.*, 1996]. Conventionally, the definition of meander belt refers to the zone between the tangents to the outsides of the curves or meanders of the active stream [*Jefferson*, 1902; *Chang and Toebes*, 1970; *Chitale*, 1970; *Allen*, 1984]. With the aim of investigating the long-term dynamics, a preferable definition would refer to a wider region of the floodplain which comprises cutoffs as well as the active channel [*Matthes*, 1941]. Accordingly, we define

as meander belt the portion of the floodplain having a probability equal to 0.90 of containing the riverbed during its long-term evolution.

[39] As expected, the spatial scale D_0 (or $\bar{\lambda}$) proves to be useful also to scale the width of meander belt defined in such a way. Figure 7a illustrates an example of the frequency of the riverbed occurrence during a simulated planimetric evolution at the steady state. Different colors distinguish the probability of recurrence. It is clear again the self-confining action of the cutoff. As shown in Figure 7b, several simulations provide the same universal width of meander belt of about $40-50D_0$, which is equivalent to about $3.0-3.8\bar{\lambda}$ (using the result $\bar{\lambda} \simeq 13.4D_0$ shown in Figure 4b). Figures 8a–8c compare the planimetry of three real rivers with the belt $3.4\bar{\lambda}$ wide (marked by the bold black lines): the agreement is remarkable and similar results are obtained for the other rivers shown in Figures 9 and 10. Notice that all the maps were rescaled by the respective value of $\bar{\lambda}$ (i.e., D_0). Because of this rescaling, the geometrical patterns of the active channel appear to be visually indistinguishable, thus confirming the scale invariance of the long-term equilibrium condition. These pictures clearly show that a meander belt equal to $3.4\bar{\lambda}$ captures most part of the oxbow lakes recorded on the floodplain. This is particularly evident where the floodplain maintains visible traces of the past river paths because of absence of agriculture (e.g., for the rivers in Alaska).

5. Conclusions

[40] The numerical simulations, supported by an extensive analysis of real data, suggest a twofold role of cutoffs in providing a statistical equilibrium to meandering rivers as well as in selecting the few fluid dynamic mechanisms governing the long-term meandering dynamics. As a consequence, two fundamental scales, D_0 and T_0, are sufficient to describe the main features of the long-term evolution. In particular, very good collapses have been obtained by the spatial scale, D_0, for several geometrical quantities. This universal behavior, obtained on fluid dynamic basis and not empirically, has been confirmed by analyzing several real rivers with very different hydraulic characteristics. The agreement between numerical simulations and statistics from real rivers also confirms the reliability of the simulations and supports the use of linear models to describe the long-term behavior of meandering rivers.

[41] The results are also in agreement with some well-known empirical geomorphological laws. In this respect, the present analysis suggests that the success of these laws, in spite of the complex fluid dynamic processes involved in the meandering dynamics, is due to the filtering action of the cutoffs and to the use of quantities directly linked to D_0 to rescale the geometric characteristics.

[42] The statistical analysis of the recurrences of the riverbed during the long-term evolution provides a probabilistic characterization of the meander belt that is in good agreement with aerial and satellite data. Although a more detailed analysis would require the comparison with geological records of the fluvial recurrence, the oxbow lake traces visually detected from maps have furnished an encouraging indication of the goodness of the proposed methodology and of its usefulness for geostatistical analysis and engineering applications.

Appendix A: Coefficients of JP Model

[43] The coefficients in equation (6) are

$$\sigma_0' = \frac{2rC_f M^2}{\nu_0 U_0 \sqrt{\theta}}, \quad \sigma_1' = \frac{b^2 C_f}{\nu_0 H_0 U_0}(3 - 2\Phi_T) + \frac{rH_0}{\nu_0 U_0 \sqrt{\theta}} \tag{A1}$$

$$\rho_0' = 2b\left[\frac{C_f r}{\sqrt{\theta}}\left(F^2 a_0 - 1\right) - k_3\sqrt{C_f}\right](-1)^m \tag{A2}$$

$$\rho_1' = 2b\left[\frac{rH_0 a_0}{\sqrt{\theta}} + \frac{rH_0 a_0 k_4}{\sqrt{C_f r}} + \frac{\beta C_f b^2}{M^2 H_0}\right](-1)^{m+1} \tag{A3}$$

$$\rho_2' = \frac{-2a_0 b^3 (-1)^m}{M^2} \tag{A4a}$$

$$r = 0.55 \tag{A4b}$$

$$F = \frac{U_0}{\sqrt{gH_0}}. \tag{A4c}$$

The expressions of a_0, Φ_T, k_3, and k_4 are reported by *Zolezzi and Seminara* [2001].

Appendix B: Numerical Computation of I_j

[44] Although the usual numerical integration methods for the efficient computation of the integral I_j in (9) is the Fast Fourier Transform, involving $O(N^2 \ln N)$ operations, its use here has some operative disadvantages. For instance, it needs to fix the number of points to a power of 2 and it is particulary sensitive to the extremes of the domain. We thus used a different numerical procedure which takes advantage of the particular exponential form of the kernel, and reduces the number of the operations to less than N^2.

[45] Consider the computation of $I_2(s)$ (the same scheme is valid also for the other integrals) and, for notational simplicity, define $I^i = I_2(s_i)$, where i (i = 1, .., N) is the sequential point at the coordinate curvilinear s_i (i.e., $i = s_i/\Delta s$). First, the interval of integration [0, s] can be truncated at [s-$a\Delta s$, s] with a negligible error provided that a is such that $e^{-\epsilon_2 a \Delta s} \ll \eta$ where η is the numerical precision. Hence, using the extended Simpson's rule and defining $f_j^i = C(j)e^{\epsilon_2 (i-j)\Delta s}$, the numerical computation of I^i can be written as

$$I^i \simeq \left(\Gamma_i + e^{\epsilon_2 i \Delta s}\sum_{j=i-a+3}^{i-3} C(j)e^{-\epsilon_2 j \Delta s}\right)\Delta s, \tag{B1}$$

where

$$\Gamma_i = \frac{3}{8}\left(f_{i-a}^i + f_i^i\right) + \frac{7}{6}\left(f_{i-a+1}^i + f_{i-1}^i\right) + \frac{23}{24}\left(f_{i-a+2}^i + f_{i-2}^i\right).$$

[46] The key point to minimize computational efforts is to compute the sum in (B1) only at the first point and, for the next points, update the sum by subtracting the first term and adding the new last term. To avoid overflow in the exponential terms, such a procedure is repeated only for limited windows of the domain with width $W < N$ (where W depends on η and ϵ). It follows that for the kth windows $i = i_k, .., i_k + W - 1$. Finally, if we multiply and divide the second term in the r.h.s. of (B1) by $e^{\epsilon_2 F \Delta s}$ with $F = i_k - 1$, at the generic kth window we obtain

$$I^i \simeq \left(\Gamma_i + e^{\epsilon_2 (i-F)\Delta s}\Phi_i\right)\Delta s, \tag{B2}$$

with

$$\Phi_i = \Phi_{i-1} + f^F_{i-3} - f^F_{i-a+3} \quad (i = i_k + 1, .., i_k + W - 1),$$

$$\Phi_{i_k} = \sum_{i_k - a + 3}^{i_k - 3} f^F_{i_k}.$$

Appendix C: Algorithm for Searching Neck Cutoff

[47] Define a grid $A(j, k)$ ($j = 1, .., J$; $k = 1, .., K$), with square cells of side equal to the cutoff threshold distance d_c. Each point i ($i = 1, .., N$) of the discretized river planimetry lies in a cell of the grid $A(j, k)$. A second matrix $B(n, m)$ ($n = 1, .., L = J \cdot K$; $m = 1, .., M = \sqrt{2} d_c/\Delta s$) is introduced as an ''address'' matrix: each cell $A_{j,k}$ corresponds to the nth row (being $n = J(k - 1) + j$) of B. Notice that, for smooth curves such as meanders, M is the maximum number of points contained in a single cell. Finally, the orthogonal coordinates (x_i, y_i) of the points i are recorded in a third matrix $C(N, 2)$ (namely $C_{i,1} = x_i$, $C_{i,2} = y_i$).

[48] Initially, the matrix B is set to zero. The first step consists in reducing the zone where cutoff is searched. For each ith row of the matrix C, the algorithm identifies the corresponding position in A, then it assigns the sequential number i, which parameterizes the curve, to the respective position of the address in B ($B_{n,1} = i$). If $B_{n,1} \neq 0$ then $B_{n,2} = i$ and so on.

[49] In the second step B is scanned and every time that a row is not zero (namely, $B_{n,m} \neq 0$ and $B_{n,m+1} = 0$), the distances between the points contained in the adjacent cells and in the cell itself are calculated, that is,

$$d_1 = \left|B_{n,m}, B_{p,1}\right|, \quad \text{with} \quad p - n = -1, 4, 5, 6, 1 \tag{C1}$$

$$d_2 = \left|B_{n,m}, B_{n,1}\right|, \quad \text{if} \quad m > 1, \tag{C2}$$

where the norm is defined as

$$|p, q| = \sqrt{\left(C_{p,1} - C_{q,1}\right)^2 + \left(C_{p,2} - C_{q,2}\right)^2}. \tag{C3}$$

[50] Finally, the cutoff condition is satisfied if $d_1 \leq d_c$ or $M\Delta s \leq d_2 \leq d_c$.

[51] The first step involves N operations, whereas the second step takes at maximum $\tau_m N \Delta s/d_c$ operations, being τ_m the maximum tortuosity occurred during the simulations. Hence, considering $\tau_m = 6$, $\Delta s = b/4$ and $d_c = 1.5b$, we obtain $6N$ total operations, rather than $N(N - 1)/2$ operations taken by a point-to-point distance evaluation.

Notation

A	lateral slope factor of the bed.
b	river half-width (m).
C	curvature (m^{-1}).
$\lvert C\rvert$	mean absolute curvature (m^{-1}).
$\tilde{C}$	dimensionless curvature.
C_f	friction factor.
C_{f0}	friction factor of the ''straightened'' river.
d_m	mean sediment diameter (m).
E	coefficient of bank erodibility.
F	Froude number.
f	Darcy-Weisbach coefficient.
g	metric coefficient of the curvilinear coordinates.
H	average flow depth (m).
H_0	average flow depth of the ''straightened'' river (m).
I	overall bed slope.
k	dimensionless river wave number defined by equation (13).
m	lateral mode of the Fourier decomposition of $u(s, n)$.
n	transversal coordinate (m).
$\mathbf{n}$	normal-to-curve versor.
Q	mean annual discharge ($m^3\ s^{-1}$).
R_0	minimum radius of curvature (m^{-1}).
$\mathbf{r}$	parameterized vector of the curve position (m).
s	arc length coordinate (m).
S	sinuosity.
t	temporal variable (s).
U	mean stream velocity ($m\ s^{-1}$).
U_0	mean stream velocity of the ''straightened'' river ($m\ s^{-1}$).
u	longitudinal flow field perturbation ($m\ s^{-1}$).
u_b	local excess bank longitudinal velocity.
u_m	m mode of the lateral decomposition of $u(s, n)$ ($m\ s^{-1}$).
V	bank erosion velocity ($m\ s^{-1}$).
$\tilde{V}$	dimensionless bank erosion velocity.
α	purely descriptive parameter of the curve independent of time (m).
β	aspect ratio.
ϵ_j	eigenvalues of the modeling equations.
ζ	normal displacement of the curve (m).
η	dimensionless bed elevation.
θ	Shield stress.
λ	linear wavelength (m).
λ_c	curvilinear wavelength (m).
$\bar{\lambda}$	spatially averaged linear wavelength (m).
$\bar{\lambda}_c$	spatially averaged curvilinear wavelength (m).
ν_0	ratio between the half-width and the minimum radius of curvature.
ρ_j	coefficients of the nonhomogeneous part of the modeling equations in the original dimensionless framework.

σ_j coefficient of the homogeneous part of the modeling equations in the original dimensionless framework.
τ tortuosity of river planimetry.
ϕ angle between the local tangent to the river axis and the x coordinate (rad).

[52] **Acknowledgments.** The authors are grateful to Eliana Perucca for her help in the simulations and to referees Chris Paola and Jim Pizzuto and one anonymous referee for their useful comments. Finally, we thank the Cassa di Risparmio di Cuneo (CRC) Foundation for financial support.

References

Allen, J. R. L. (1984), *Sedimentary Structures: Their Character and Physical Basis*, Elsevier, New York.
Argyris, J., G. Faust, and M. Haase (1994), *An Exploration of Chaos*, *Texts Comput. Mech.*, vol. 7, Elsevier, New York.
Beck, S. (1984), Mathematical modelling of meander interaction, in *River Meandering*, edited by C. M. Elliott, pp. 932–941, Am. Soc. of Civil Eng., New York.
Beck, S., D. A. Melfi, and K. Yalamanchili (1984), Lateral migration of the Genesses River, New York, in *River Meandering*, edited by C. M. Elliott, pp. 510–517, Am. Soc. of Civil Eng., New York.
Brower, R. C., D. A. Kessler, J. Koplik, and H. Levine (1984), Geometrical models of interface evolution, *Phys. Rev. A*, *29*, 1335–1342.
Carlston, C. W. (1965), The relation of free meander geometry to stream discharge and its geomorphic implications, *Am. J. Sci.*, *263*, 864–885.
Chang, T. P., and G. H. Toebes (1970), A statistical comparision of meander planforms in the Wabash basin, *Water Resour. Res.*, *6*, 557–578.
Chitale, S. V. (1970), River channel patterns, *J. Hydraul. Div. Am. Soc. Civil Eng.*, *96*(1), 201–221.
Dean, R. B. (1974), Reynolds number dependence on skin friction in two dimensional rectangular duct flow and a discussion on the law of the Wake, *IC Aero. Rep. 74-11*, Imperial Coll. of Sci. and Technol., London.
Do Carmo, M. (1976), *Differential Geometry of Curves and Surface*, Prentice-Hall, Upper Saddle River, N. J.
Edwards, B. F., and D. H. Smith (2002), River meandering dynamics, *Phys. Rev. E*, *65*, 046303.
Furbish, D. J. (1991), Spatial autoregressive structure in meander evolution, *Geol. Soc. Am. Bull.*, *103*(12), 1576–1589.
Gagliano, S. M., and P. C. Howard (1984), The neck cutoff oxbow lake along the lower Mississippi river, in *River Meandering*, edited by C. M. Elliot, pp. 147–158, Am. Soc. of Civil Eng., New York.
Hansen, E. (1967), On the formation of meanders as a stability problem, *Prog. Rep. 13*, Coastal Eng. Lab., Tech. Univ. of Denmark, Lyngby, Denmark.
Howard, A. D. (1984), Simulation model of meandering, in *River Meandering*, edited by C. M. Elliott, pp. 952–963, Am. Soc. of Civil Eng., New York.
Howard, A. D. (1992), Modeling channel migration and floodplain sedimentation in meandering streams, in *Lowland Floodplain Rivers: Geomorphological Perspectives*, edited by P. A. Carling and G. E. Petts, pp. 1–41, John Wiley, Hoboken, N. J.
Howard, A. D., and A. T. Hemberger (1991), Multivariate characterization of meandering, *Geomorphology*, *4*, 161–186.
Ikeda, S. G., G. Parker, and K. Sawai (1981), Bend theory of river meanders: 1. Linear development, *J. Fluid Mech.*, *112*, 363–377.
Jansen, P., L. Van Bendegom, J. Van Den Berg, M. de Vries, and A. Zanen (1979), *Principles of River Engineering: The Non Tidal Alluvial River*, Pitman, London.
Jefferson, M. S. W. (1902), Limiting width of meander belts, *Natl. Geogr. Mag.*, *13*, 373–384.
Johannesson, H., and G. Parker (1989), Linear theory of river meanders, in *River Meandering*, *Water Resour. Monogr.*, vol. 12, edited by S. Ikeda and G. Parker, pp. 181–214, AGU, Washington, D. C.
Kantz, H., and T. Schreiber (1997), *Nonlinear Time Series Analysis*, Cambridge Univ. Press, New York.
Leopold, L. B., and M. G. Wolman (1960), River meanders, *Bull. Geol. Soc. Am.*, *71*, 769–794.
Leopold, L. B., M. G. Wolman, and J. P. Miller (1964), *Fluvial Processes in Geomorphology*, W. H. Freeman, San Francisco, Calif.
Liverpool, T. B., and S. F. Edwards (1995), Dynamics of a meandering river, *Phys. Rev. Lett.*, *75*(16), 3016–3019.
Matthes, G. H. (1941), Basic aspects of stream meanders, *Eos Trans. AGU*, *22*, 632–636.
Nakayama, K., H. Segur, and M. Wadati (1992), Integrability and the motion of curves, *Phys. Rev. Lett.*, *69*(18), 2603–2606.
Nikora, V., V. B. Sapozhnikov, and D. A. Noever (1993), Fractal geometry of individual river channels and its computer simulation, *Water Resour. Res.*, *29*, 3561–3568.
Odgaard, A. J. (1986), Meander flow model. I: Development, *J. Hydraul. Eng.*, *112*(12), 1117–1136.
Parker, G. (1976), On the cause and characteristic scales of meandering and braiding in rivers, *J. Fluid Mech.*, *76*, 457–483.
Parker, G., and E. D. Andrews (1986), On the time development of meanders bends, *J. Fluid Mech.*, *162*, 139–156.
Parker, G., and H. Johannesson (1989), Observations on several recent theories of resonance and overdeepening in meandering channels, in *River Meandering*, *Water Resour. Monogr.*, vol. 12, edited by S. Ikeda and G. Parker, pp. 379–415, AGU, Washington, D. C.
Parker, G., P. Diplas, and J. Akiyama (1983), Meanders bends of high amplitude, *J. Hydraul. Eng. Am. Soc. Civil Eng.*, *109*(10), 1323–1337.
Perona, P., A. Porporato, and L. Ridolfi (2002), River dynamics after cutoff: A discussion of different approaches, in *Proceedings of the River Flow 2002 International Conference on Fluvial Hydraulics*, edited by D. Bousmar and Y. Zech, pp. 715–721, Int. Assoc. for Hydraul. Res., Madrid, Spain.
Perucca, E., C. Camporeale, and L. Ridolfi (2005), Nonlinear analysis of the geometry of meandering rivers, *Geophys. Res. Lett.*, *32*, L03402, doi:10.1029/2004GL021966.
Pizzuto, J., and T. Meckelnburg (1989), Evaluation of a linear bank erosion equation, *Water Resour. Res.*, *25*, 1005–1013.
Seminara, G. (1998), Stability and morphodynamics, *Meccanica*, *33*, 59–99.
Seminara, G., M. Tubino, and D. Zardi (1994), Planimetric evolution of meandering rivers from incipient formation to cutoff (in Italian), paper presented at XXIV Convegno di Idraulica e Costruzioni Idrauliche, Cons. Naz. delle Ric, Naples, Italy, 20–22 Sept.
Seminara, G., G. Zolezzi, M. Tubino, and D. Zardi (2001), Downstream and upstream influence in river meandering. part 2. Planimetric development, *J. Fluid. Mech.*, *438*, 213–230.
Snow, R. S. (1989), Fractal sinuosity of streams channels, *Pure Appl. Geophys.*, *131*, 99–109.
Stølum, H. H. (1996), River meandering as a self-organized process, *Science*, *271*, 1710–1713.
Stølum, H. H. (1997), Fluctuations at the self-organized critical state, *Phys. Rev. E.*, *56*, 6710–6718.
Stølum, H. H. (1998), Planform geometry and dynamics of meandering rivers, *Am. Bull. Geol. Soc.*, *110*(11), 1485–1498.
Sun, T., T. Jøssang, P. Meakin, and K. Schwarz (1996), A simulation model for meandering rivers, *Water Resour. Res.*, *32*, 2937–2954.
Sun, T., P. Meakin, and T. Jøssang (2001), A computer model for meandering rivers with multiple bed load sediment size: 1. Theory, *Water Resour. Res.*, *37*, 2227–2241.
Swanson, D. C. (1993), The importance of fluvial processes and related reservoir deposits, *J. Pet. Technol.*, 368–377.
Zolezzi, G., and G. Seminara (2001), Downstream and upstream influence in river meandering. Part 1. General theory and application to overdeepening, *J. Fluid Mech.*, *438*, 183–211.

C. Camporeale and L. Ridolfi, Department of Hydraulics, Politecnico di Torino, Corso Duca degli Abruzzi 24, I-10129, Torino, Italy. (carlo.camporeale@polito.it)

P. Perona, Institute of Hydromechanics and Water Resources Management, ETH, Wolfgang-Pauli-Str. 15, CH-8093 Zurich, Switzerland.

A. Porporato, Department of Civil and Environmental Engineering, Duke University, 127 Hudson Hall, Box 90287, Durham, NC 27708-0328, USA.